

J.W. NICHOLSON^{1,✉}
A.K. ABEELUCK²
C. HEADLEY²
M.F. YAN¹
C.G. JØRGENSEN³

Pulsed and continuous-wave supercontinuum generation in highly nonlinear, dispersion-shifted fibers

¹ OFS Laboratories, 600–700 Mountain Avenue, Murray Hill, NJ 07974, USA

² OFS Laboratories, 25 Schoolhouse Road, Somerset, NJ 08873, USA

³ OFS Fitel Denmark I/S, Priorparken 680, 2605 Brøndby, Denmark

Received: 5 February 2003/Revised version: 25 April 2003
Published online: 24 June 2003 • © Springer-Verlag 2003

ABSTRACT Supercontinuum generation in a highly nonlinear, dispersion-shifted fiber at 1550 nm is discussed. Spectrum generation under both pulsed and continuous-wave conditions is considered. With a few meters of highly nonlinear, dispersion-shifted fiber and a femtosecond erbium fiber laser, an octave-spanning supercontinuum is demonstrated. Kilometer lengths of nonlinear fiber pumped by a continuous-wave Raman fiber laser are shown to generate a continuum with a bandwidth greater than 247 nm. A nonlinear Schrödinger-equation model is used to investigate the effect of varying the dispersion on the pulsed continuum and noise effects in the continuous-wave continuum.

PACS 42.81.Dp; 42.65.Wi; 42.55.Wd

1 Introduction

Supercontinuum generation has been a subject of numerous investigations for years, see e.g. [1], both because of the interesting nonlinear physics that takes place during the continuum-generation process, as well as the many applications of supercontinuum sources. In particular, recent demonstrations of supercontinuum generation in microstructured fibers have sparked renewed interest in continuum generation in optical fibers [2–4]. Spectra with spans greater than an octave have been generated by propagating femtosecond pulses from solid-state lasers through these small-core fibers, and can be used for measuring and stabilizing the pulse to pulse carrier-envelope phase and as high-precision optical frequency combs [5, 6]. Other applications for supercontinuum from fibers include optical coherence tomography [7], spectrally sliced sources for wavelength-division multiplexing (WDM) communication systems [8–11], and as high-power, low-noise sources for device characterization [12, 13].

Silica, with a nonlinear index $n_2 = 2.36 \times 10^{-20} \text{ m}^2/\text{W}$, is by no means a particularly high nonlinearity material. In spite of this situation, the long interaction lengths available in optical fibers allow for impressive nonlinear effects. Much work has gone towards increasing the nonlinearity available in silica optical fibers through the use of the high index contrast

and small core that can be achieved in microstructured fibers. In spite of the increased nonlinearity achieved in microstructured fibers, however, there are advantages in investigating nonlinear properties of fibers made by standard doping of silica with germanium and fluorine.

A relatively new type of germanium-doped silica fiber with low dispersion slope and a small effective area has recently been developed [14]. Careful design of the index profile allows the fiber to achieve a small effective area and low dispersion and dispersion slope, while maintaining low loss. These fibers have nonlinear coefficients several times that of standard transmission fibers, and are often referred to as highly nonlinear, dispersion-shifted fibers, or simply HNLFs. HNLF is compatible with standard telecom components, and can be fusion spliced with low loss to standard single-mode fiber (SMF). Typical splice losses for SMF to HNLF are 0.2 dB at 1550 nm in this work, although we have demonstrated splice losses as low as 0.01 dB. Furthermore, HNLF can be low loss compared to highly nonlinear microstructured fibers; for HNLF used in these experiments the measured attenuation was between 0.7 and 1.1 dB/km at 1550 nm. In addition, by altering the diameter of the fiber during draw slightly, a range of dispersion values from negative to positive at 1550 nm can be achieved.

The HNLF dispersion slope can be very low; the slope for fibers used in these experiments was $0.024 \text{ ps nm}^{-2} \text{ km}^{-1}$ at 1550 nm. The effective area of the HNLF, $A_{\text{eff}} \approx 10\text{--}13.9 \mu\text{m}^2$ at 1550 nm, and the nonlinear coefficient, $\gamma \approx 8.5\text{--}10 \text{ W}^{-1} \text{ km}^{-1}$, were calculated from the measured index profile. The nonlinear coefficient γ for HNLF is several times that of standard single-mode fiber.

Both pulsed and continuous-wave (cw) laser sources can be built from integrated, all-fiber components. Mode-locked erbium fiber lasers can deliver high-quality sub-100-fs pulses [15], while high-power, cascaded Raman fiber lasers (RFLs) pumped by cladding-pumped Yb fiber lasers can deliver several watts of cw power at a range of wavelengths [16]. The ability to directly splice HNLF with low loss to the output of fiber lasers to create integrated, all-fiber continuum sources operating in a range of regimes is therefore a useful advantage.

Several different pump sources have been used to demonstrate supercontinuum in microstructured and tapered fibers. For example, Cr:forsterite lasers operating at $1.25 \mu\text{m}$ [17] and tunable pulses from optical parametric amplifiers in the

✉ E-mail: jwn@ofsoptics.com

range from 1.3 to 1.5 μm [18, 19] have successfully demonstrated continuum generation in silica and non-silica fibers. However, most of the work in continuum generation in microstructured fibers has centered around 800 nm. Therefore, in Sect. 2 we make a comparison between continuum generation with a Ti:sapphire laser in a microstructured fiber and continuum generation with a pulsed erbium fiber laser in HNLF. In Sect. 2.1 we present measurements of pulsed continuum generation at 1550 nm in HNLF. To generate these spectra, lengths of HNLF a few meters long are typically used. We experimentally investigate the role of HNLF dispersion, and show that, by altering the dispersion along the length of the HNLF, the continuum can span more than an octave. In Sect. 2.2 we present a numerical model of the continuum generation at 1550 nm based on the nonlinear Schrödinger equation (NLSE).

Because of the high peak powers required for continuum generation, relatively little work has concentrated on cw sources (see e.g. [20, 21]). However, the advent of high-power cw fiber lasers has opened the possibility of cw continuum sources in compact, all-fiber devices. While the bandwidth from cw sources is less than that from pulsed sources, the average power can be considerably higher. In Sect. 3.1 we present a high-average-power, all-fiber cw continuum source based on a Raman fiber laser and HNLF. In contrast to the pulsed experiments, kilometer lengths of HNLF are required to generate the cw continuum. In Sect. 3.3 we present a simple model of the cw continuum generation, based again on the nonlinear Schrödinger equation.

2 Pulsed continuum generation in HNLF

Efforts at modeling the continuum in microstructured fibers generated by pulsed solid-state lasers are generally based on a modified nonlinear Schrödinger equation, and have aimed at understanding the fundamental processes involved in the spectrum generation [22–27]. The relationship between the generating pulse wavelength and the fiber dispersion for a Ti:sapphire laser and an air–silica microstructured fiber is illustrated in Fig. 1. The dispersion curves are calculated from measured fiber index profiles. The broadest continuum is generated when the laser pulse is in the anomalous-dispersion regime of the fiber. The pulse initially begins to self-Raman shift to longer wavelengths. As these higher-order solitons break up, parametric four-wave mixing

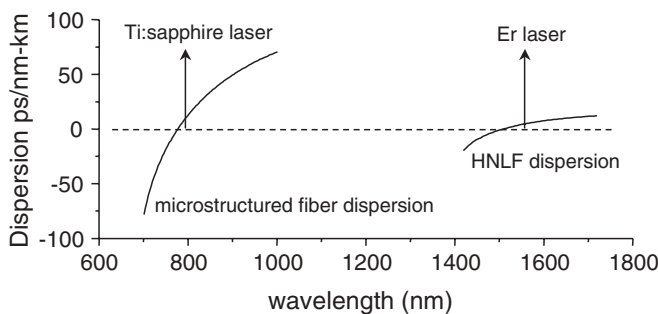


FIGURE 1 Dispersion of a typical small-core microstructured fiber in relation to the Ti:sapphire wavelength compared to HNLF dispersion and an Er fiber laser

generates frequencies at wavelengths shorter than the zero-dispersion wavelength.

Figure 1 shows that the relationship between an erbium laser's wavelength and HNLF dispersion is similar to a Ti:sapphire/microstructured fiber system, shifted to longer wavelengths. Therefore, one would expect the interplay between a 1550-nm pulse, launched into an anomalous-dispersion HNLF, and a nearby dispersion zero to generate the same extreme supercontinuum, as confirmed in recent experiments [28, 29]. Although the different values for fiber parameters, such as the low dispersion slope seen in Fig. 1 for HNLF, or the much higher nonlinear coefficient γ achieved in microstructured fibers, makes modeling of each individual system critical, it is important to remember that the same underlying generation process governs continuum generation in both microstructured fiber and HNLF.

2.1 Experimental setup

The experimental setup is shown in Fig. 2. The laser was a passively mode-locked erbium fiber laser [15], with a repetition rate of 33 MHz and an average power of 7 mW, centered at 1550 nm. A retrieval from an amplitude-unbalanced, interferometric correlation plus the pulse spectrum [30] showed an intensity FWHM of 188 fs. To boost the average power, the pulses were stretched in negative-dispersion fiber (HSDK, OFS Denmark), amplified in an erbium amplifier, and re-compressed in positive-dispersion, standard single-mode fiber. Alternatively, for low-power experiments, the pulses from the oscillator were launched directly into the HNLF. We obtained average powers up to 50 mW, although at these power levels significant self-phase modulation was observed at the output of the positive-dispersion fiber.

The optical spectrum from 1 μm to 1.77 μm was observed with an optical spectrum analyzer (OSA) (ANDO model AQ-6315B). For wavelengths longer than 1.77 μm , the optical spectrum was measured using a scanning monochromator and a thermoelectric-cooled PbS detector. In the region from 1.5 μm to 1.77 μm the spectra from the two devices were compared, showing good agreement.

Lengths of HNLF with different dispersion were drawn from the same preform by changing the fiber diameter slightly during the draw. Spectra generated by pulses directly from the laser oscillator in 10 m of 2.2 ps nm⁻¹ km⁻¹ dispersion HNLF as a function of launch power are shown in Fig. 3a. The spectra have been offset vertically for clarity. The sharp spikes in the spectrum at -2 dB m are soliton sidebands from

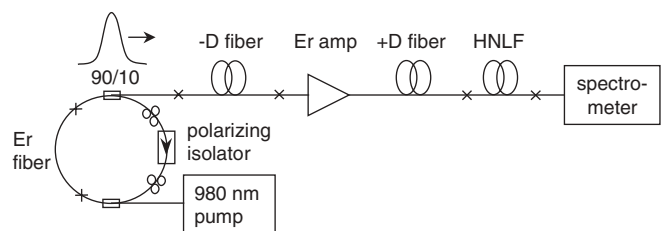


FIGURE 2 Experimental setup for pulsed supercontinuum generation in HNLF at 1550 nm

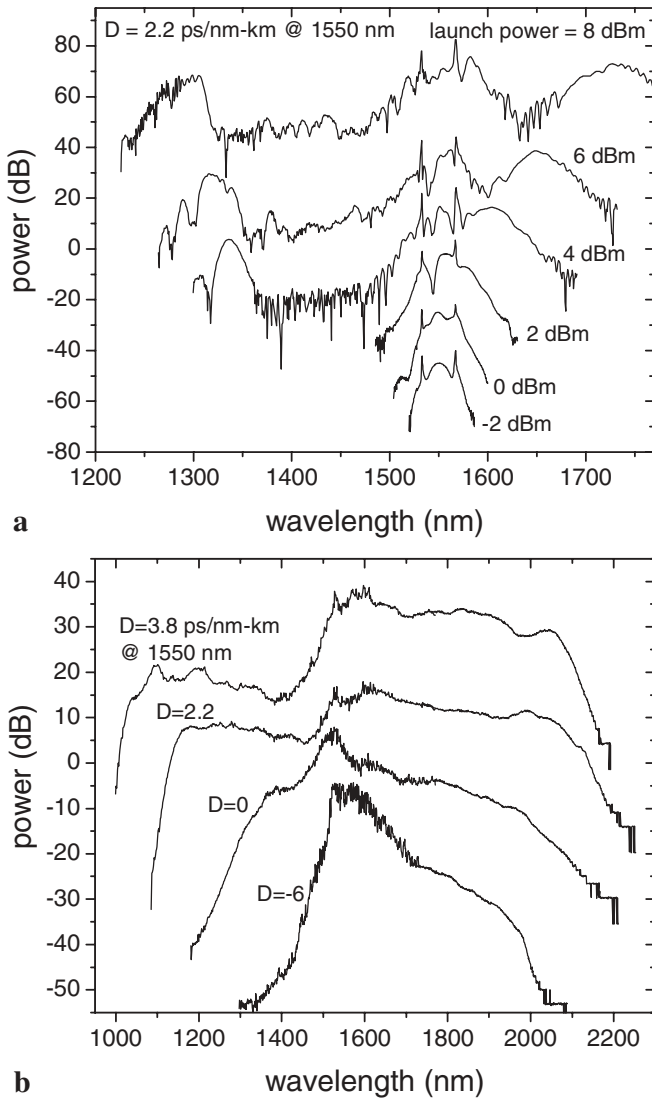


FIGURE 3 a Supercontinuum at low powers in 10 m of $2.2 \text{ ps nm}^{-1} \text{ km}^{-1}$ dispersion HNLF. b Supercontinuum in 10-m lengths of HNLF as a function of dispersion at 1550 nm

the laser oscillator itself [31]. Polarization-maintaining fiber was not used in these experiments. As the power is slowly increased a self-Raman-shifted pulse can be seen breaking off from the main pulse. As the launch power is increased further, a second pulse appears to break off and new components corresponding to four-wave mixing (FWM) frequencies appear at wavelengths shorter than the zero-dispersion wavelength of 1460 nm . This is the same basic sequence of events observed and predicted theoretically for microstructured fiber continuum at 800 nm .

The spectrum as a function of dispersion for 50-mW average power is shown in Fig. 3b. At these powers, much of the structure observed at low power has disappeared. The narrowest spectra are observed for negative dispersion at 1550 nm . As the dispersion is increased, the spectrum becomes broader, but the relative power at wavelengths below zero dispersion becomes weaker. HNLF lengths as long as 600 m were tested. At these lengths, the shoulder at short wavelengths was substantially filled in. However, the short-wavelength edge of

the spectrum was not extended any further, and the long-wavelength edge of the spectrum was attenuated at wavelengths past $2 \mu\text{m}$ due to linear loss in the fibers. As well as being extremely broad, interference measurements have shown that the coherence of the continuum can be maintained during the generating process [32].

Generating continuum with ps pulses in kilometer lengths of fiber, in which the dispersion decreases along the length of the fiber, can generate broader and flatter continuum due to adiabatic soliton compression [10, 33]. While it is difficult to tune the dispersion during draw for such short (meter) lengths of fiber, we have found that HNLF can be fusion spliced to itself with 0.02-dB loss. Therefore, arbitrary dispersion maps can be designed by splicing together different-diameter sections of HNLF.

We constructed a 6-m hybrid HNLF fiber consisting of four 1.5-m sections of HNLF with different dispersions. The dispersion decreased from one end of the hybrid fiber to the other, with the four sections having a dispersion at 1550 nm of, in order, $3.8, 2.2, 0, \text{ and } -2 \text{ ps nm}^{-1} \text{ km}^{-1}$. Figure 4 shows the spectra generated by launching into the two different ends of the fiber with 50 mW of average power. In addition, the continuum generated by the 10-m fiber with $D = 3.8 \text{ ps nm}^{-1} \text{ km}^{-1}$ is shown for comparison purposes.

The continuum generated by launching into the positive-dispersion end of the hybrid fiber spanned from $1.073 \mu\text{m}$ to $2.311 \mu\text{m}$ at the 20-dB point. At the point down 15 dB from the peak, the continuum spanned more than an octave. The hybrid-fiber spectrum is substantially broader and flatter than that generated by the $3.8 \text{ ps nm}^{-1} \text{ km}^{-1}$ fiber, even though the hybrid fiber is 4-m shorter, a result consistent with continuum generation by ps pulses in kilometer lengths of dispersion-decreasing fiber [33].

Launching into kilometer lengths of dispersion-decreasing fiber with picosecond pulses results in an adiabatic compression of solitons and a broader, flatter continuum [10, 33]. In contrast, launching into the negative-dispersion end of the fiber initially leads to pulse broadening and a narrower con-

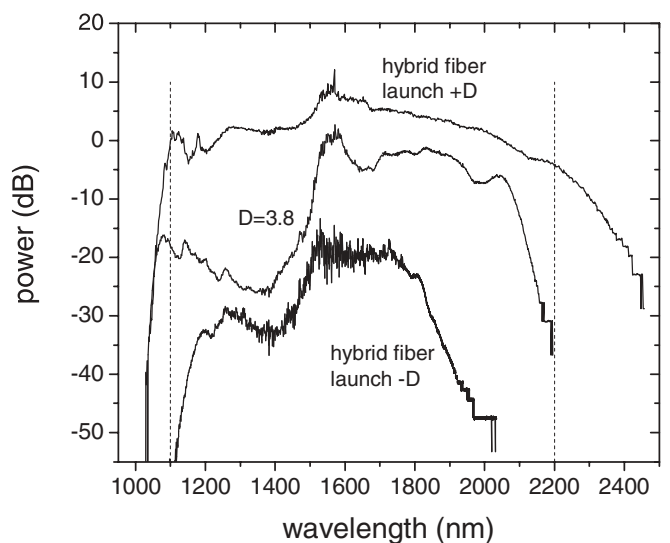


FIGURE 4 Supercontinuum generated from 10 m of $D = 3.8 \text{ ps nm}^{-1} \text{ km}^{-1}$ dispersion fiber compared to the 6-m hybrid-fiber supercontinuum

tinium. These effects are identical to those observed in the 6-m hybrid fiber. The nonlinear Schrödinger-equation model, discussed in Sect. 2.2, is used to understand the enhancements seen in the hybrid-fiber continuum.

2.2 Nonlinear Schrödinger-equation model of pulsed continuum generation

A generalized nonlinear Schrödinger equation has been used successfully to explain many of the features seen in propagation of high-power pulses in fibers [22–26]. The equation

$$\begin{aligned} \frac{\partial E(z, t)}{\partial z} = & -\frac{\alpha}{2} E - \left[\sum_{m=2} \beta_m \frac{i^{m-1}}{m!} \frac{\partial^m}{\partial t^m} \right] E \\ & + i\gamma (1 - f_R) \left[|E|^2 E - \frac{2i}{\omega_0} \frac{\partial}{\partial t} (|E|^2 E) \right] \\ & + i\gamma f_R \left[1 + \frac{i}{\omega_0} \frac{\partial}{\partial t} \left\{ E \int_0^\infty h_R(t') |E(z, t-t')|^2 dt' \right\} \right] \end{aligned} \quad (1)$$

includes the effects of linear loss and dispersion (first and second terms on the right-hand side of (1)), self-phase modulation and self-steepening (third and fourth terms), and the delayed Raman effect (final term). The equation is solved by a modified split-step method [34]. Here, $E(z, t)$ is the electric field as a function of propagation distance z and time t , α is the linear loss, β_m are the linear dispersion coefficients, γ is the effective nonlinearity, and ω_0 is the center angular frequency. The relative contributions of the instantaneous and delayed Raman effects is given by f_R and the Raman response function is given by $h_R(t)$ [34]. Measured dispersion, nonlinearity, and loss values are used in the simulations.

A comparison between experimental measurements and the numerical model of the continuum generation at low average power is shown in Fig. 5. Figure 5a shows the measured spectrum after the 6-m-long hybrid fiber as well as a 10-m length of $D = 2.2 \text{ ps nm}^{-1} \text{ km}^{-1}$ dispersion fiber. The average power was 1 mW, with a peak power of approximately 150 W. As discussed above, the hybrid fiber shows significantly more spectral broadening than the constant-dispersion fiber. Figure 5b shows the numerical simulations corresponding to the experimental conditions, with the measured pulse spectrum used as the initial condition for the model, assuming a flat spectral phase. There is excellent agreement between the experiment and the model, with most of the detailed spectral features in the experiment being reproduced in the numerical simulations.

At high launch powers, it is far more difficult to obtain such a close comparison between simulations and experiments because of the extreme sensitivity of the fine spectral features to the initial pulse chirp, power, and launch polarization. However, the over-all trends in the experiment are also observed in the numerical model. Figure 6 shows a simulation of the continuum generated in a 10-m length of $D = 3.8 \text{ ps nm}^{-1} \text{ km}^{-1}$ constant-dispersion fiber compared to the 6-m hybrid fiber for 6.5-mW average power, or a peak power of 1 kW. The spectra have been offset for clarity. In

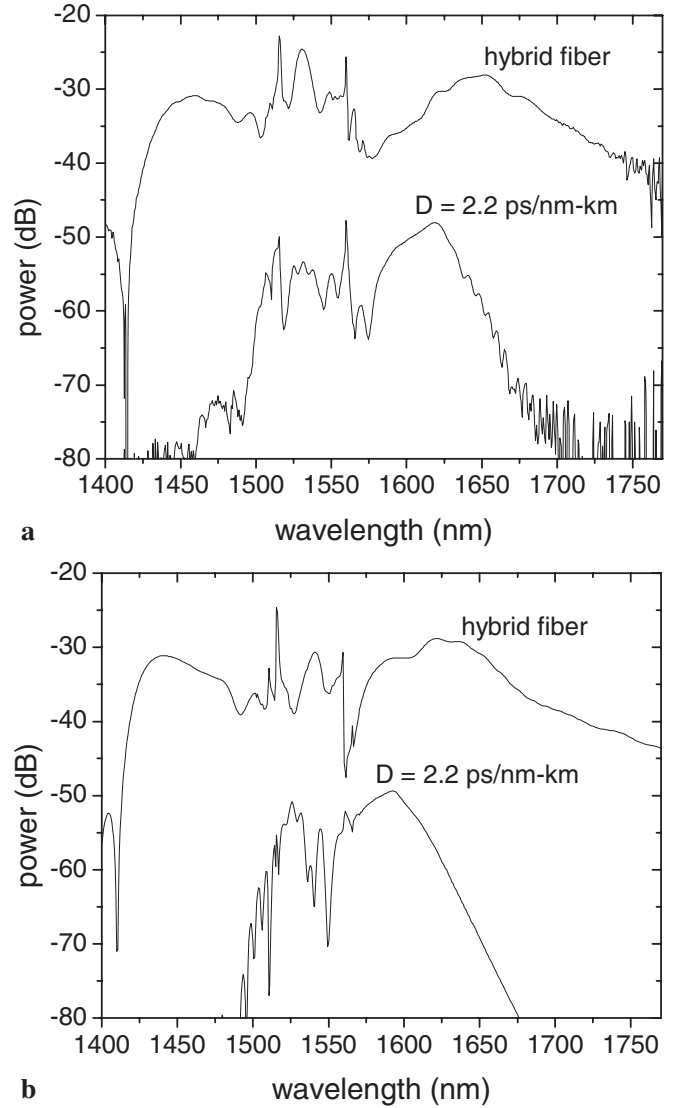


FIGURE 5 Comparison of **a** experimental measurements and **b** numerical simulations of spectral broadening in the $D = 2.2 \text{ ps nm}^{-1} \text{ km}^{-1}$ fiber and the hybrid fiber at 1-mW average power

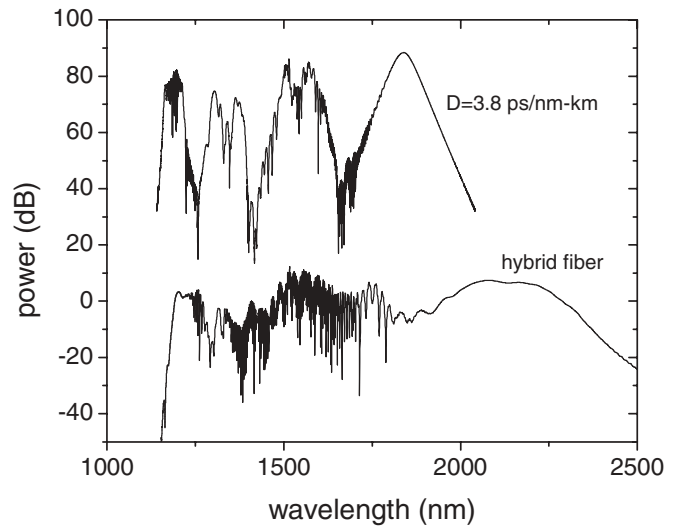


FIGURE 6 Numerical simulation of continuum generation in 10-m $D = 3.8 \text{ ps nm}^{-1} \text{ km}^{-1}$ fiber compared to 6-m hybrid fiber for 1-kW peak-power launch

agreement with the experiment, the simulations show much more spectral broadening in the hybrid fiber compared to the constant-dispersion fiber, as well as a much flatter continuum from the hybrid fiber.

Figure 7 shows the calculated evolution of the pulse peak power as a function of propagation distance for three different HNLFs. Previous numerical simulations of continuum generation in microstructured fiber at 800 nm have shown that the initial stage of propagation is marked by strong pulse compression [27]. The same behavior is observed in our numerical simulations at 1550 nm in HNLF, and correspondingly the peak power initially increases dramatically in all the fiber types with positive dispersion.

In the fibers with constant dispersion, the initial increase in peak power is followed by a slow monotonic decrease. In the time domain, a Raman soliton is observed to break off and self-Raman shift to longer wavelengths, as observed in the experimental measurements in Fig. 3a. This Raman soliton also shows a slow increase in FWHM (plotted in the inset of Fig. 7) after the initial stage of pulse compression.

The peak power as a function of propagation distance is observed to have a very different behavior in the hybrid fiber. As the pulse enters successive fiber sections with smaller dispersion, the Raman soliton again shows a decrease in FWHM and an increase in peak power. When the peak power again begins to decrease, it is still maintained at a higher level than it would be in the constant-dispersion fiber alone. This process repeats itself in each new section of the hybrid fiber, resulting in a compressed Raman soliton with a higher peak power and a shorter FWHM than is generated in any of the constant-dispersion fibers.

Figure 7 also shows that in the hybrid fiber, as currently designed, the Raman soliton has not frequency shifted sufficiently by the time it reaches the final fiber ($D = -2 \text{ ps nm}^{-1} \text{ km}^{-1}$ at 1550 nm) to be in the anomalous-dispersion regime. Consequently the pulses stretch in the

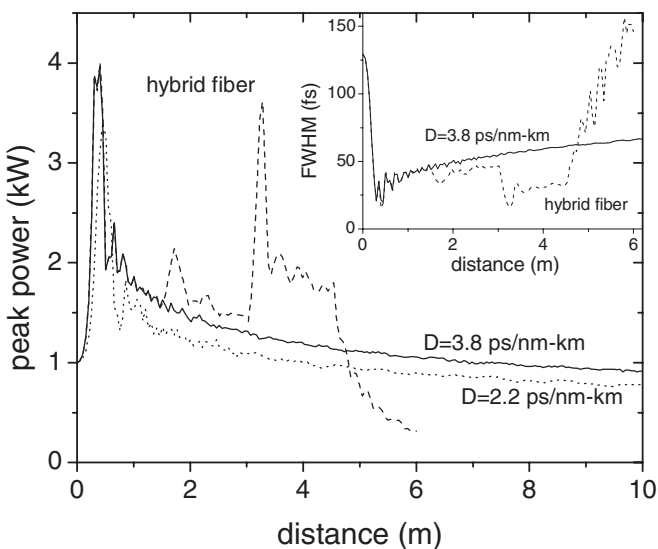


FIGURE 7 Peak power as a function of propagation distance in the $D = 3.8 \text{ ps nm}^{-1} \text{ km}^{-1}$ HNLF, $D = 2.2 \text{ ps nm}^{-1} \text{ km}^{-1}$ fiber, and hybrid fiber. *Inset*: full width at half maximum of the main Raman soliton as a function of propagation distance

last fiber stage, and the bulk of the continuum generation is achieved in the first 4.5 m of HNLF.

3 CW continuum generation in HNLF

Most of the work to date on the topic of supercontinuum generation has dealt with supercontinua seeded by pulsed sources with high peak powers. As shown in Sect. 2.1, octave-spanning bandwidths can be achieved with pulsed sources, but the average power was a few tens of milliwatts. The average power of the continuum can be increased by using high-power continuous-wave (cw) lasers such as Raman fiber lasers (RFLs). High-power supercontinuum generation was recently demonstrated by Prabhu et al. in a cw Brillouin/Raman fiber laser [20]. The continuum had a bandwidth of 100 nm and was centered at about 1483.4 nm. In this paper, supercontinuum generation over the same bandwidth is demonstrated experimentally in 1 km of HNLF with a cw RFL pump at 1596 nm. The full potential of the source is then shown by generating a supercontinuum with a bandwidth greater than 247 nm in 4.5 km of HNLF. In both cases, the pump is positioned in the anomalous-dispersion regime.

3.1 Experimental setup

The experimental configuration for studying continuum generation in the HNLF is shown in Fig. 8a. The pump source was a diode-pumped RFL with a tunable band-pass filter in the cavity, allowing the output wavelength (λ_p) to be varied from 1570 to 1600 nm. Details of the tunable RFL are shown in Fig. 8b. The outputs of laser diodes emitting at 915 nm were multiplexed to pump a 1485-nm cascaded Raman resonator (CRR). The output of the CRR was then divided through a 3-dB coupler to co- and counter-pump a 2-km length of Raman fiber in a ring cavity to generate light of the next Stokes shift. The ring cavity incorporated an isolator, a band-pass filter (BPF) to provide wavelength selectivity,

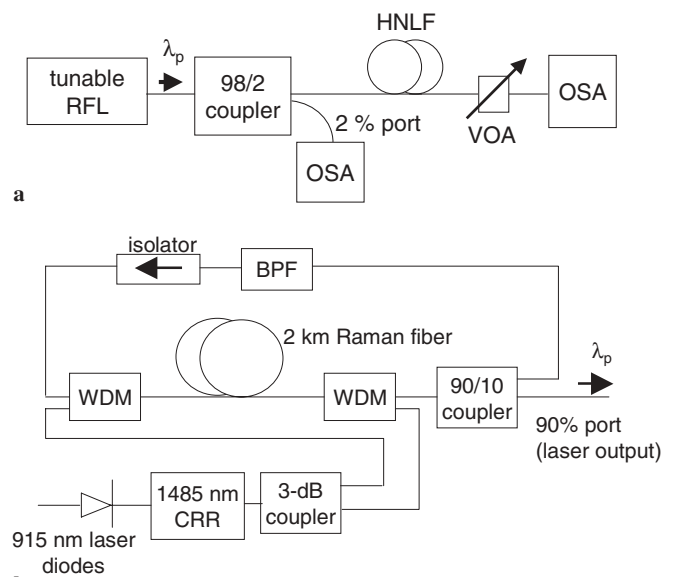


FIGURE 8 **a** Experimental setup for supercontinuum generation in a HNLF using a cw Raman fiber laser pump and **b** details of the tunable Raman fiber laser

and two wavelength-division multiplexers (WDMs) to combine the 1485-nm light from the CRR and the Stokes light generated in the cavity. The output of the tunable laser was available through the 90% port of a 90/10 coupler in the ring cavity.

The output from the tunable RFL was launched into a 1-km length of HNLF via a 98/2 coupler, the 2% output port of which was used to monitor the power fluctuation of the pump source using an optical spectrum analyzer (OSA), as shown in Fig. 8a. The output from the HNLF was attenuated using a variable optical attenuator (VOA) and monitored with a second OSA. The HNLF used in the experiment had a zero-dispersion wavelength (λ_0) close to 1594 nm. Spectra of the continuum were acquired as a function of the power launched into the HNLF and also as a function of the pump wavelength. The OSA resolution was 0.05 nm.

3.2 Results and discussion

Figure 9a and c shows the input and output spectra as a function of launch power when the pump wavelength was in the anomalous-dispersion regime ($\lambda_p > \lambda_0$). The input and output spectra when the pump was in the normal-dispersion regime ($\lambda_p < \lambda_0$) are plotted in Fig. 9b and d, respectively. The 1485-nm line shown in the input spectra is the residual light coming from the Raman fiber laser pump itself. Additional weaker lines are also present at longer wavelengths. In the anomalous-dispersion regime, shown in Fig. 9c, with a pump

centered at 1596 nm and a launch power of 904 mW, the 20-dB bandwidth (measured from the peak of the pump laser) of the continuum is 100 nm, spanning a wavelength range from 1568 nm to 1668 nm. In comparison, the 20-dB bandwidth of the corresponding input spectrum shown in Fig. 9a is only 2.8 nm. Moreover, the measured average power of the broad continuum is 503 mW for an initial launch power of 904 mW. The continuum showed good long-term stability with a maximum standard deviation in power of only 0.5 dB over a period of 70 min. During the same time period, the maximum standard deviation of the pump power across its 20-dB bandwidth was 0.33 dB [21].

Continuum generation in the anomalous-dispersion regime can be accounted for by a combination of stimulated Raman scattering (SRS) and parametric gain due to four-wave mixing (FWM). The effect of SRS only can be seen in Fig. 9d, where the pump is positioned in the normal-dispersion regime at $\lambda_p = 1575$ nm. A broad Stokes peak becomes visible at 1693 nm and grows as the input pump power is increased. When the pump is positioned in the anomalous-dispersion regime at $\lambda_p = 1596$ nm, shown in Fig. 9c, the growth of a similar Stokes wave also occurs, but is now accompanied by FWM. Spectral broadening due to degenerate FWM, for instance, can be calculated from the dispersion properties of the fiber and by considering the following condition on the phase mismatch, κ , in the single-mode HNLF [34] (neglecting the small contribution of the phase mismatch due to waveguiding),

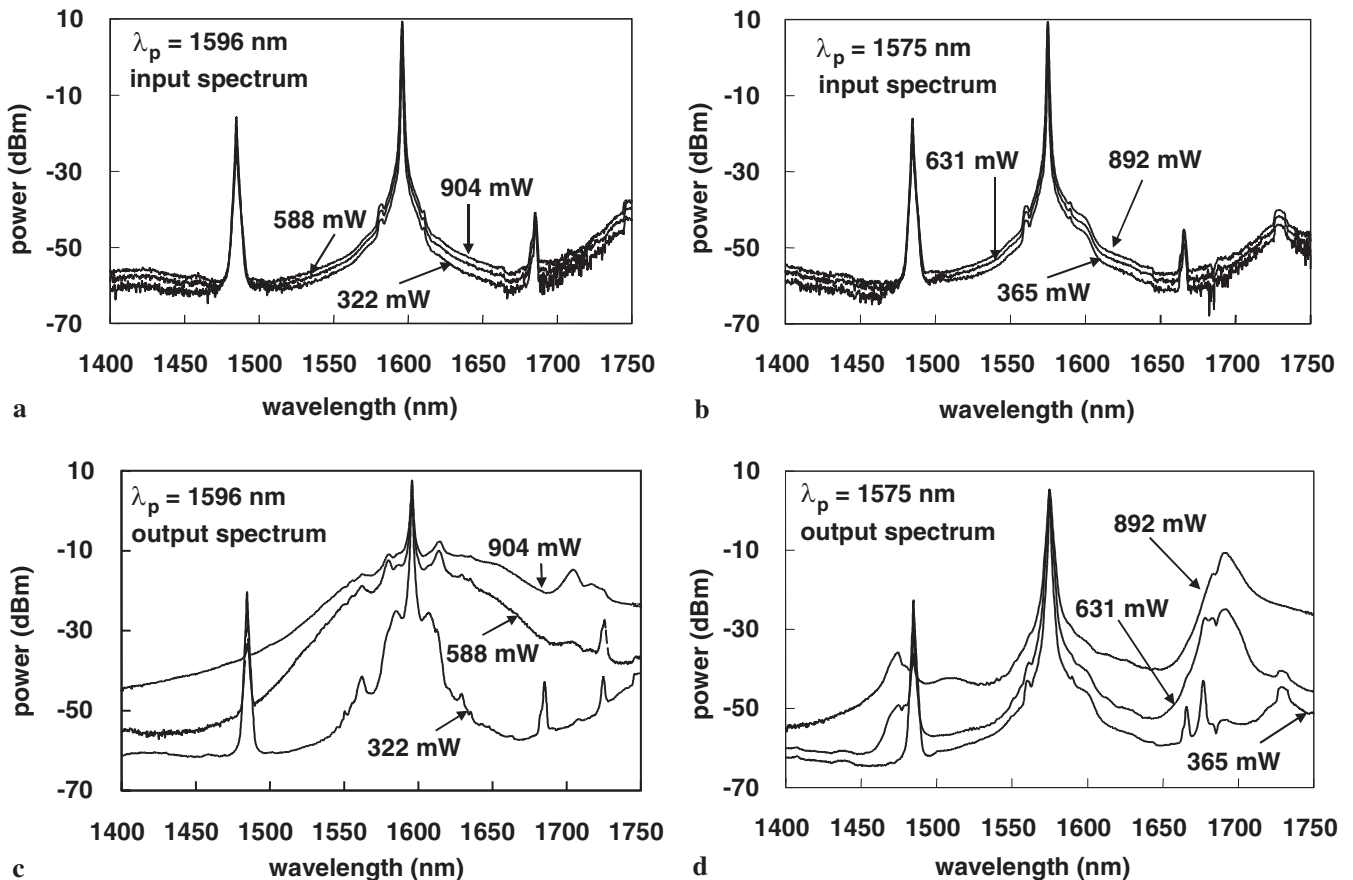


FIGURE 9 Input spectra for a $\lambda_p = 1596$ nm and b $\lambda_p = 1575$ nm as a function of launch power. c, d Corresponding output spectra from 1 km of HNLF

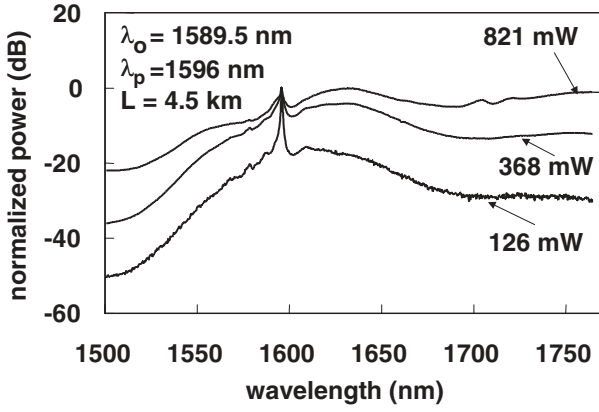


FIGURE 10 Supercontinuum generation in 4.5 km of HNLF as a function of launch power with the pump at 1596 nm. The power along the vertical axis has been normalized with respect to the maximum power across the spectrum for each trace

$$\kappa = \sum_{n=1}^{\infty} \frac{2\beta_{2n}}{(2n)!} \Omega_s^{2n} + 2\gamma P_0 = 0, \quad (2)$$

where β_{2n} is the $2n$ th-order dispersion coefficient at the pump wavelength, Ω_s is the frequency shift, γ is the effective nonlinearity, and P_0 is the total input power. Unlike the normal-dispersion regime, phase matching (and, hence, efficient FWM) in the anomalous-dispersion regime is ensured by the balance between the negative contribution of material dispersion and the positive contribution of fiber nonlinearity. The sidebands appearing on opposite sides of the pump wavelength in Fig. 9c can be interpreted as the result of FWM phase matched by self-phase modulation (also referred to as modulation instability). The combined effect of SRS and FWM is responsible for the large gain that is observed in the anomalous-dispersion regime as the launch power is increased.

The experiment was repeated with a 4.5-km length of HNLF. The growth of the supercontinuum as a function of launch power is shown in Fig. 10. The fiber has a λ_0 of 1589.5 nm. The pump was positioned in the anomalous-dispersion regime at $\lambda_p = 1596$ nm, as before. The increased redistribution of the pump power over the supercontinuum is seen by the decrease in power at 1596 nm relative to the background supercontinuum. The effect is more pronounced in Fig. 10 compared to the results shown in Fig. 9c, where only 1 km of HNLF was used. Measurements for wavelengths greater than 1770 nm were not made using the PbS detector. Nevertheless, Fig. 10 shows that a bandwidth greater than 247 nm and an output power greater than 210 mW were achieved by pumping the HNLF with 821 mW of power. By using a HNLF with a shorter λ_0 , a supercontinuum spanning the S, C, and L bands could be generated using a single pump source.

3.3 Modeling cw continuum generation with the NLSE

We again return to (1) to investigate the processes behind cw continuum generation. Modeling of the cw case with the NLSE is decidedly more difficult than in the pulsed case, because of the large time and frequency windows required. Although it is difficult to match experimental condi-

tions exactly in the model, a certain insight can be gained from the simulations.

Long pulses whose frequency spectrum is much narrower than the modulation instability gain peak have been used in the past experimentally as quasi-cw inputs [35], and this approach is used here. Super-Gaussian pulses 400 ps in length with $m = 10$ were used as a quasi-cw input to the simulation. The HNLF dispersion zero was assumed to be at 1550 nm, and the power was set to 1 W. The noise-free input pulse is shown in Fig. 11 as a solid line. When this pulse was propagated through 2 km of HNLF at 1552 nm, almost no change in spectrum was observed. In contrast, a Gaussian pulse ($m = 1$) with a peak power of 1 W showed spectral broadening from self-phase modulation. From these results it was concluded that the assumption of a cw input for these power levels for the super-Gaussian pulse was adequate.

The fiber lasers used in the cw experiments show high levels of relative-intensity noise (RIN). Therefore, it was the goal of this simulation to investigate the influence of RIN on the continuum-generation process. An example of the super-Gaussian pulse with RIN added is shown as a dotted line in Fig. 11.

The spectrum output from 2 km of HNLF when the launched wavelength is 1545 nm is shown in Fig. 12a. The spectrum at the start of the simulation is shown for reference in the inset, on the same wavelength scale. Very little spectral broadening is observed. In contrast, when the launched wavelength is in the anomalous-dispersion regime, significant spectral broadening is observed for a noisy input (Fig. 12b). For reference, the inset in Fig. 12b shows the output from 2 km of HNLF for a noise-free input.

The NLSE is an excellent model for various nonlinear effects in pulse propagation, but cw simulations are challenging. Furthermore, notably missing from the model as it stands now is spontaneous Raman scattering. Nevertheless, the simulations show that noise on cw lasers operating in the anomalous-dispersion regime can serve as a strong seed for cw continuum generation, and broad spectra can be generated from the efficient phase-matched FWM at power levels easily attainable in Raman fiber lasers.

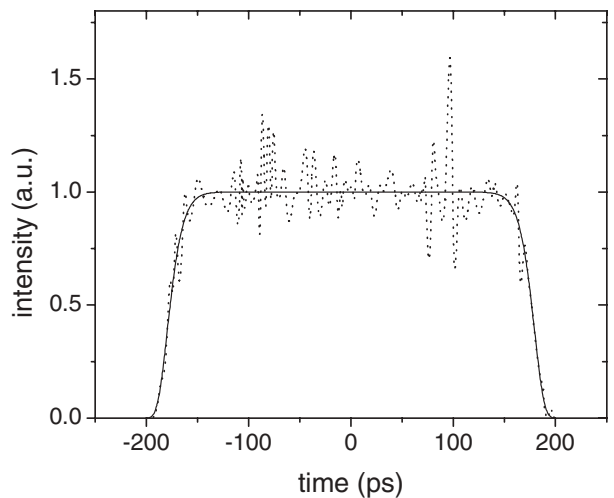


FIGURE 11 Super-Gaussian ($m = 10$) pulse used as a quasi-cw input to the NLSE. Solid line: noise-free input. Dotted line: noisy input

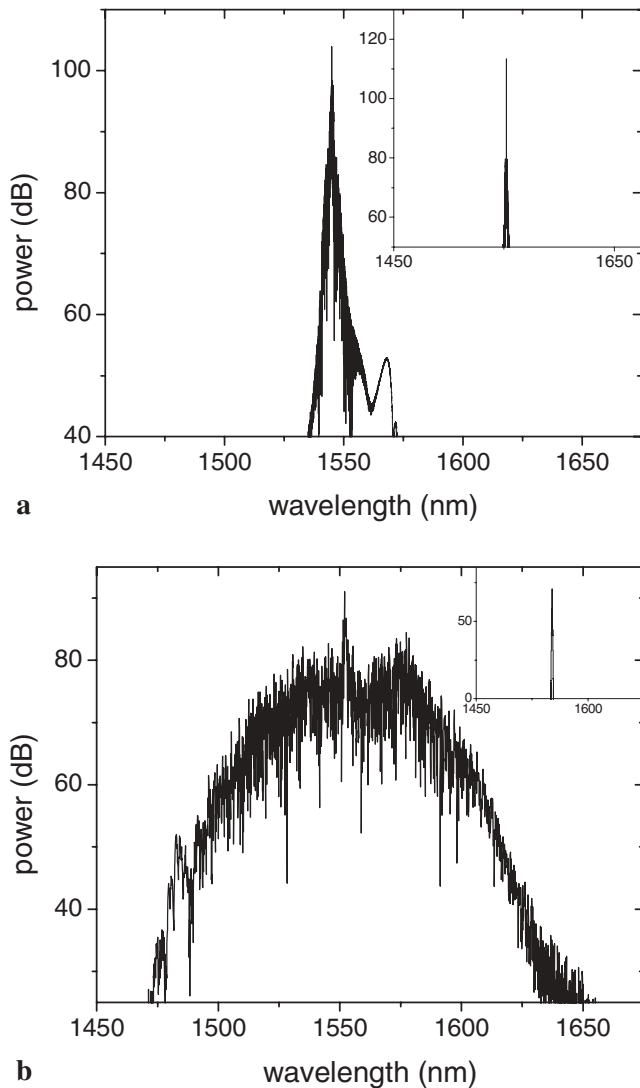


FIGURE 12 Simulation output spectrum for a noisy input when the launched wavelength is **a** 1545 nm (*inset* = launched spectrum) and **b** 1552 nm (*inset* = output for noise-free input). Dispersion zero was 1550 nm. *Insets* are shown on the same wavelength scales as main plots

4 Conclusions

With meter-long lengths of HNLF spliced to a femtosecond erbium laser, continua showing the same characteristics as those generated at 800 nm in microstructured fiber were demonstrated. Furthermore, the ability to fusion splice different-diameter HNLFs made possible a hybrid HNLF fiber in which the dispersion decreased along the length of the fiber. This hybrid fiber showed a broader and flatter continuum than constant-dispersion HNLF, and the behavior of the hybrid fiber was well modeled by a nonlinear Schrödinger calculation. Using the hybrid fiber we were able to produce over an octave of bandwidth, which is, to the best of our knowledge, the broadest continuum generated in an all-fiber source at 1550 nm.

Using kilometer lengths of HNLF coupled with a cw Raman fiber laser, high-average-power cw continuum was demonstrated. A supercontinuum with a bandwidth greater than 247 nm was generated by pumping 4.5 km of a HNLF

with a cw Raman fiber laser. Again, to the best of our knowledge, this is the broadest supercontinuum generated to date using a cw pump. Finally, NLSE modeling of a quasi-cw input showed that RIN is a strong seed for the continuum generation with high-power cw lasers.

Although the nonlinear coefficient of HNLF is not as high as microstructured or non-silica fibers, the low loss, the variety of dispersion values that can be achieved, and the ability to fusion splice HNLF to fiber lasers to make integrated-fiber continuum sources make HNLF a useful and versatile fiber.

REFERENCES

- 1 R.R. Alfano (Ed.): *The Supercontinuum Laser Source* (Springer, Berlin 1989)
- 2 J.K. Ranka, R.S. Windeler, A.J. Stentz: *Opt. Lett.* **25**, 25 (2000)
- 3 T.A. Birks, W.J. Wadsworth, P.S.J. Russell: *Opt. Lett.* **25**, 1415 (2000)
- 4 R. Holzwarth, M. Zimmermann, T. Udem, T.W. Hänsch, P. Russbuldt, K. Gäbel, R. Poprawe, J.C. Knight, W.J. Wadsworth, P.S.J. Russell: *Opt. Lett.* **26**, 1376 (2001)
- 5 M. Bellini, T.W. Hänsch: *Opt. Lett.* **25**, 1049 (2000)
- 6 D.J. Jones, S.A. Diddams, J.K. Ranka, A. Stentz, R.S. Windeler, J.L. Hall, S.T. Cundiff: *Science* **288**, 635 (2000)
- 7 I. Hartl, X.D. Li, C. Chudoba, R.K. Ghanta, T.H. Ko, J.G. Fujimoto, J.K. Ranka, R.S. Windeler: *Opt. Lett.* **26**, 608 (2001)
- 8 Y. Takushima, F. Futami, K. Kikuchi: *IEEE Photon. Technol. Lett.* **10**, 1560 (1998)
- 9 T. Morioka, S. Kawanishi, K. Mori, M. Saruwatari: *Electron. Lett.* **30**, 1166 (1994)
- 10 T. Okuno, M. Onishi, M. Nishimura: *IEEE Photon. Technol. Lett.* **10**, 72 (1998)
- 11 C.X. Yu, H.A. Haus, I.P. Ippen, W.S. Wong, A. Sysoliatin: *Opt. Lett.* **25**, 1418 (2000)
- 12 F. Koch, S.V. Chernikov, J.R. Taylor: *Opt. Commun.* **175**, 209 (2000)
- 13 J. Jasapara, R. Bise, R. Windeler: In *Tech. Dig. Optical Fiber Communications Conf.*, 2002 (OSA, Washington, DC 2002) pp. 519–521
- 14 T. Okuno, M. Onishi, T. Kashiwada, S. Ishikawa, M. Nichimura: *IEEE J. Sel. Top. Quantum Electron.* **5**, 1385 (1999)
- 15 K. Tamura, E.P. Ippen, H.A. Haus, L.E. Nelson: *Opt. Lett.* **18**, 1080 (1993)
- 16 S. Grubb, T. Erdogan, V. Mizrahi, T. Strasser, W.Y. Cheung, W.A. Reed: In *Proc. Optical Amplifiers and Their Applications 1994*, p. 187
- 17 A.B. Fedotov, A.N. Naumov, A.M. Zheltikov, I. Bugar, J.D. Chorvat, D. Chorvat, A.P. Tarasevitch, D. von der Linde: *J. Opt. Soc. Am. B* **19**, 2156 (2002)
- 18 D.A. Akimov, A.A. Ivanov, M.V. Alfimov, S.N. Bagayev, T.A. Birks, W.J. Wadsworth, P.J. Russell, A.B. Fedotov, F.S. Pivtsov, A.A. Podshivalov, A.M. Zheltikov: *Appl. Phys. B* **74**, 307 (2002)
- 19 V.V.R.K. Kumar, A.K. George, W.H. Reeves, J.C. Knight, P.S.J. Russell, F.G. Omenetto, A.J. Taylor: *Opt. Express* **10**, 1520 (2002)
- 20 M. Prabhu, N.S. Kim, K. Ueda: *Jpn. J. Appl. Phys.* **39**, L291 (2000)
- 21 A.K. Abeeluck, S. Radic, K. Brar, J.-C. Bouteiller, C. Headley: In *Tech. Dig. Optical Fiber Communications Conf.*, 2003 (OSA, Washington, DC 2003) pp. 561–562
- 22 K.J. Blow, D. Wood: *IEEE J. Quantum Electron.* **QE-25**, 2665 (1989)
- 23 A.L. Gaeta: *Opt. Lett.* **27**, 924 (2002)
- 24 J.M. Dudley, S. Coen: *Opt. Lett.* **27**, 1180 (2002)
- 25 A.V. Husakov, J. Hermann: *Phys. Rev. Lett.* **87**, 203901 (2001)
- 26 S. Coen, A.H.L. Chau, R. Leonhardt, J.D. Harvey, J.C. Knight, W.J. Wadsworth, P.S.J. Russell: *J. Opt. Soc. Am. B* **19**, 753 (2002)
- 27 B.R. Washburn, S.E. Ralph, R.S. Windeler: *Opt. Express* **10**, 575 (2002)
- 28 N. Nishizawa, T. Goto: *Jpn. J. Appl. Phys.* **40**, L365 (2001)
- 29 J.W. Nicholson, M.F. Yan, P. Wisk, J. Fleming, F. DiMarcello, E. Monberg, A. Yablon, C. Jørgensen, T. Veng: *Opt. Lett.* **28**, 643 (2003)
- 30 J.W. Nicholson, W. Rudolph: *J. Opt. Soc. Am. B* **19**, 330 (2002)
- 31 M.L. Dennis, I.N. Duling III: *Appl. Phys. Lett.* **62**, 2911 (1993)
- 32 J. Nicholson, M. Yan, A. Yablon, P. Wisk, J. Fleming, F. DiMarcello, E. Monberg: In *Tech. Dig. Optical Fiber Communications Conf.*, 2003 (OSA, Washington, DC 2003) pp. 511–512
- 33 K. Mori, H. Takara, S. Kawanishi, M. Saruwatari, T. Morioka: *Electron. Lett.* **33**, 1806 (1997)
- 34 G.P. Agrawal: *Nonlinear Fiber Optics*, 2nd edn. (Academic, London 1995)
- 35 K. Tai, A. Hasegawa, A. Tomita: *Phys. Rev. Lett.* **56**, 135 (1986)